Table 2. Average numbers of the most relevant secondary particles exiting the 30 cm long, 1.5 cm diameter mercury target per incident proton (FLUKA). The μ^+/μ^- numbers and the K^+/K^0 numbers have been multiplied by 10^4. Note that the K^- production rate is at the level of 10^{-5} per incident proton.

E_k (GeV)	p	n	γ	e^-	e^+	π^+	π^-	μ^+	μ^-	K^+	K^0
2.2	1.4	17	5.0	0.17	0.08	0.24	0.18	4	1	7	6
3.5	1.8	23	7.0	0.28	0.15	0.41	0.37	10	3	35	30
4.5	2.3	25	7.7	0.35	0.21	0.57	0.39	11	3.3	93	68
8	3.1	33	11.0	0.63	0.41	1.00	0.85	30	9.5	413	340

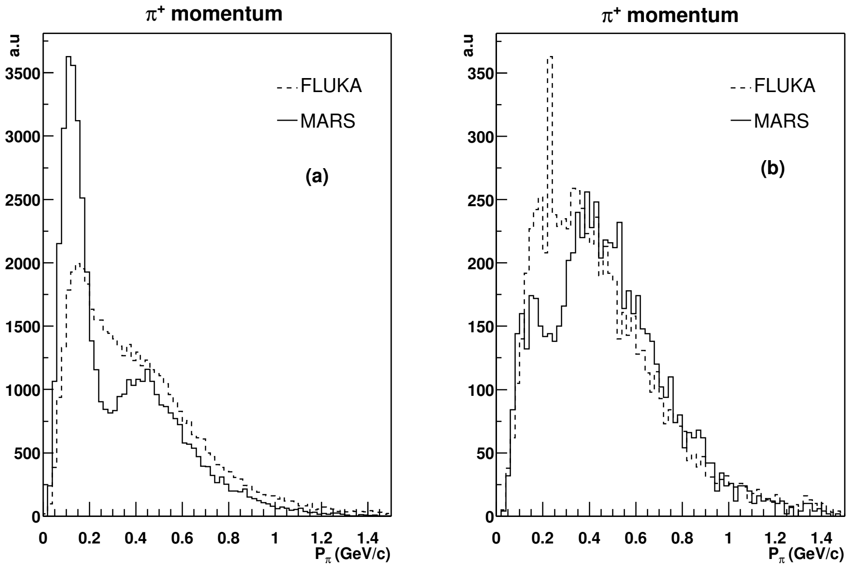

Figure 2. Pion momentum distribution at the exit of the target (a) and at the exit of the horns (b), simulated by FLUKA (- - - -) and by MARS (——).

the target, computed with the two simulator programs FLUKA and MARS, is shown on figure 2(a). Pions come from Δ decays which in turn are originated from two different sources. At low energy ($P < 200$ MeV/c), Δ are produced by protons of the target excited by the beam interactions, while the highest energy part of the spectrum is due to transformation of protons of the beam into Δ. The discrepancy is quite large for the low energy part. However, the horns are designed to focus the high energy part of the spectrum (see section 4), and therefore, MARS and FLUKA are in better agreement for the energy spectrum computed at the entrance of the decay tunnel, as shows figure 2(b). So, the discrepancy at low energy between MARS and FLUKA does not matter too much for the present application.

The momentum spectra of the different energies studied are plotted on figure 3(a). The distributions are normalized to 1 second, keeping constant the beam power to 4 MW. It is interesting to notice that the number of pion at 600 GeV/c is almost the same for all the energies. The difference comes from the angular distribution of

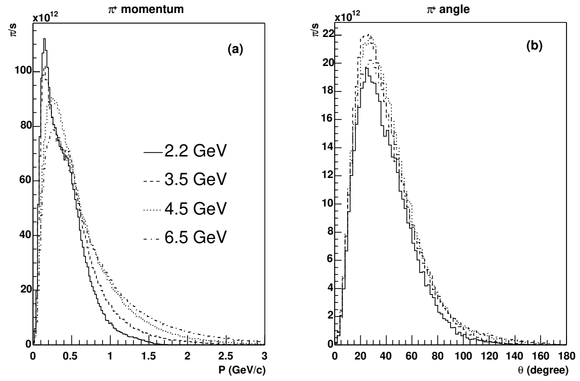

Figure 3. (a) π^+ momentum distribution at the exit of the target for the different proton beam energies studied, and (b) π^+ angular distribution of the pion having a momentum between 0.5 GeV/c and 0.7 GeV/c. (——) 2.2 GeV, (- - - -) 3.5 GeV, (······) 4.5 GeV and (— · —) 6.5 GeV.

the pion having a momentum between 0.5 GeV/c and 0.7 GeV/c (figure 3(b)) that enhance the number of interesting pion for the 3.5 GeV and 4.5 GeV proton beam.

3. Kaon production

The possibility to increase the SPL energy in order to study the optimization of the physics program has been recently pointed out [29]. Then, the kaon production should be clearly addressed because it is a source of ν_e and $\bar{\nu}_e$ background events. The kaon decay channels and branching ratios are presented in table A2 in Appendix A.3.

The target simulation described in section 2 has been used with 10^6 p.o.t with kinetic energy uniformly distributed between 2.2 GeV and 5 GeV. The momentum of outgoing pions and kaons are recorded when they exit the target. The number of produced $K^{o,\pm}$ at different proton beam energies are presented on figure 4(a). In one hand the K^o production rate is similar to the K^+ production rate, but in an other hand the K^- production rate is almost forty times smaller. For comparison, the numbers of π^+ and π^- produced in the same conditions are presented on figure 4(b). Pion production rate is about two orders of magnitude greater than the kaon production rate.

The behavior of the two pion and kaon production rates are quite different. The π^+ yield grows smoothly with the proton energy while the production of kaons seams to have two origins, which has been confirmed by FLUKA's authors [32]. For beam energy below approximatively 4 GeV, the resonance production model is used, and one notices a low production rate with a maximum at about 3.4 GeV. For beam energy above 4 GeV, the dual parton model is used, and the production rate experiences a threshold effect with a rapid rise. The ratio between positive kaon and pion production rates is about 0.5% between 2.2 GeV and 4 GeV and grow up to 2.3% at 5 GeV. One notices that the maching between the two kaon production models may not be optimal.